

Fractional Quantum Hall Effect in the Second Landau Level: the Importance of Inter-Composite-Fermion Interaction

Csaba Tóke, Michael R. Peterson, Gun Sang Jeon, and Jainendra K. Jain

Department of Physics, 104 Davey Laboratory, The Pennsylvania State University, Pennsylvania, 16802

Exact diagonalization of a two-dimensional electron gas in a strong magnetic field in the disk geometry shows that there exists a filling factor range in the second Landau level where the states significantly differ from those in the lowest Landau level. We show that the difference arises because the interaction between composite fermions is not negligible in higher Landau levels, as indicated by a substantial mixing between composite-fermion Landau-like levels, or Λ -levels. We find that the exact ground state is well reproduced by composite fermion theory with Λ -level mixing incorporated at the lowest level of approximation. Using the same variational approach in the spherical geometry we estimate the excitation gap at filling $1/3$ in the second Landau level (which corresponds to $7/3$ of experiment).

I. INTRODUCTION

A two-dimensional electron system (2DES) in a high magnetic field and low temperature exhibits a rich structure of phases as a function of the filling factor $\nu = \rho hc/eB$ (ρ is the electron density and B is the magnetic field). The integral quantum Hall effect (IQHE)¹ is characterized by quantized plateaus in the Hall resistance, where $\rho_{xy} = h/ne^2$, and a vanishing longitudinal magnetoresistance ρ_{xx} around $\nu \approx n$. This phenomenon occurs because the 2DES at integer filling factors $\nu = n$ is an incompressible liquid with a finite excitation gap. The fractional quantum Hall effect (FQHE)² refers to plateaus at $\rho_{xy} = h/fe^2$ in the vicinity of $\nu \approx f$, where f is a fraction. Our understanding of the physics of the lowest Landau level (LLL) has evolved greatly in the last two decades. The FQHE has been explained by the composite fermion (CF) theory^{3,4} as the IQHE of quasiparticles called CF's, which are electrons bound to an even number ($2p$) of quantized vortices of the many-body wave function. CF's feel a reduced magnetic field $B^* = B - 2p\rho\phi_0$, where $\phi_0 = hc/e$ is the magnetic flux quantum. Composite fermions form Landau-like levels in the reduced magnetic field, which we will call Λ -levels (Λ 's). Λ -levels are analogous to Landau levels (LL's) of electrons at B^* . (The Λ -levels have been called CF-quasi-Landau levels in the literature. To avoid confusion with the Landau levels of electrons, we prefer to use Λ -levels. "Landau level" will refer below exclusively to *electronic* Landau levels. Composite fermions can fill many Λ -levels within one Landau level.) When CF's fill an integral number n of Λ -levels, an incompressible quantum liquid with a finite excitation gap results, producing an IQHE of CF's. Such conditions are achieved at electron fillings $\nu = n/(2pn \pm 1)$, which are precisely the prominently observed fractions. Further, the microscopic wave functions based on this physics provide an excellent account of the actual eigenfunctions. CF theory with neglected inter-CF interaction thus successfully explains most of the observed fractions in the LLL.

This paper is concerned with fractional quantum Hall effect in the 2nd LL. Given that more than 50 fractions

have been observed in the lowest LL, one might expect a large number of fractions in the second LL as well, but FQHE is relatively scarce in the second or higher LL's. However, with improved experimental conditions (higher mobilities and lower temperatures), many fractions have been observed outside of the LLL. As seen in the experiments of Xia *et al.*⁵, the observed fractions are $\nu^{(1)} = 1/3, 1/5, 2/5, 2/3$, and $4/5$, where $\nu^{(1)}$ is the filling factor of the second LL. (The total filling factor is $\nu = 2 + \nu^{(1)}$ or $\nu = 3 + \nu^{(1)}$, with each LL contributing two to the filling factor, taking the spin degree of freedom into account.) Gervais *et al.*⁶ have also seen evidence for FQHE at $1/5$ and $4/5$ in the *third* LL. Indeed, the decreasing stability of CF formation has been suggested on theoretical grounds⁷, and charge-density wave phases are known to be dominant in $n \geq 2$ LL's⁸. The competition between many nearly degenerate ground states is illustrated by the observation of the so-called re-entrant integral quantum Hall effect: the system goes back and forth between the IQHE and the FQHE state several times (see, for example Eisenstein *et al.*⁹ and Xia *et al.*⁵), with the re-entrant IQHE interpreted in terms of a localization of a correlated bubble crystal proposed theoretically by Koulakov, Fogler, and Shklovskii⁸.

Because the observed fractions are consistent with the expectation from a trivial generalization of the CF theory to the second LL, it is natural to attempt an explanation in terms of composite fermions. However, the microscopic description of the observed fractions in the 2nd LL has not been as successful as in the lowest LL. As noted by Haldane¹⁰ and by d'Ambrumenil and Reynolds¹¹, a generalization of the Laughlin wave function for the ground state at $\nu = 1/3$ to the 2nd LL¹² has rather poor overlaps with the exact second LL ground state (from 0.47 to 0.61 for $4 \leq N \leq 9$ particles), which is to be contrasted with near unity overlaps in the lowest LL. In fact, exact diagonalization studies^{10,11} on small systems have been unable to capture conclusively the incompressibility of $\nu^{(1)} = 1/3$, because the system is compressible for some particle numbers and incompressible for others, and for the incompressible states, the gap varies widely with the number of particles¹¹. The observation of many

FQHE states in the filling factor range $2 < \nu < 4$ has motivated us to seek a better quantitative understanding of the FQHE in the second LL.

Another motivation arises, interestingly, from certain new FQHE states within the lowest Landau level. Pan *et al.*¹³ have observed several fractions (4/11, 5/13, 6/17, 4/13, 5/17, 7/11) that fall outside the primary Jain sequences $\nu = n/(2pn \pm 1)$. Although these sequences exhaust the possible fractions for a system of *noninteracting* composite fermions, the residual interaction between the CF's can generate more fractions, in perfect analogy to the appearance of the FQHE for electrons because of the Coulomb interaction. The new fractions are interpreted in terms of the *higher* Λ -level *fractional* QHE of composite fermions^{3,13,14,15,16,17,18}. In particular, $\nu = 4/11$ is related to the FQHE at $\nu^* = 4/3$ of CF's, i.e., $1/3$ of CF's in the second CF Λ L. (In sufficiently high magnetic fields the system is fully polarized, and electrons or composite fermions can be taken to be effectively "spinless." This is equivalent to the limit in which the Zeeman energy is much larger than the cyclotron energy. The filling factor $\nu^{(1)}$ in the second LL corresponds to $\nu = 1 + \nu^{(1)}$ for spinless electrons, but to $\nu = 2 + \nu^{(1)}$ for the real "spinful" electrons of experiment.) It was shown by Chang and Jain¹⁶ that the actual 4/11 state is extremely well described quantitatively by analogy to the $1/3$ state in the *second* LL, but not to the $1/3$ state in the lowest LL. That further underscores the need for a better quantitative understanding of the FQHE in the second LL.

Wójs and Quinn¹⁹ have argued that the difference between the LLL and the 2nd LL physics is due to some kind of pairing in the 2nd LL. They study the occupation number of various relative angular momentum m channels in the exact ground states for $8 \leq N \leq 14$ electrons in the spherical geometry and find that as the filling factor is varied (tuned by the monopole strength Q in the spherical geometry, which corresponds to $2Q$ flux quanta penetrating the surface of the sphere), there are peaks in the occupation of the $m = 5$ channel at certain flux values that they identify with $\nu = 7/3, 5/2, 8/3$. These findings are taken as evidence for pairing of electrons in the $m = 5$ channel. Wójs and Quinn thus assign a qualitatively different physics to FQHE in the second LL than that in the lowest LL, as reflected in the fact that, in the spherical geometry, their paired state at $1/3$ in the second LL occurs at the LL degeneracy $N_d = 3N - 4$ as opposed to $N_d = 3N - 2$ for the $1/3$ state in the lowest LL. (The LL degeneracy is related to the monopole strength Q by $N_d = 2Q + 3$ in the second LL.) No explicit wave functions have been constructed for the conjectured paired states which can be compared to the exact wave functions. It is noted that the likely explanation for the FQHE at $\nu = 5/2$ ²⁰ is based on the notion of pairing of composite fermions^{21,22,23,24} described by a Pfaffian wave function of Moore and Read²⁵.

Our approach is different. We attribute the same *qualitative* physics to the odd-denominator FQHE in the lowest and the second LL's (the half filled LL state behaves

very differently in the two LL's) and argue that the *quantitative* differences arise because of substantial Λ -level mixing in the second LL. The Λ -level mixing is a signature of the residual interaction between CF's. The negligibility of Λ L mixing for the lowest LL FQHE states is taken to imply that the CF's are weakly interacting. We will see that composite fermions are more strongly interacting in a range of filling factor in the second LL, although not so strongly as to destabilize all FQHE completely. The pairing at $5/2$ is already recognized as a consequence of a weak attractive interaction between composite fermions.

The higher LL FQHE has also been investigated by Goerbig, Lederer and Morias-Smith²⁶ using the Murthy-Shankar formulation of composite fermions²⁷. They do not consider Λ L mixing in their approach.

We will restrict electrons to the second LL and neglect any LL mixing. (In practice, we map the second LL problem into an effective lowest LL problem, and work within the LLL.) The Λ L mixing is treated perturbatively by diagonalizing the full Hamiltonian within a correlated basis which includes the "unperturbed" CF ground state as well as the "unperturbed" particle-hole pair excitations across Λ -levels. This is called CF diagonalization. The resulting ground state incorporates Λ L mixing, and can be improved perturbatively by inclusion of successively higher energy CF excitons. With minimal Λ L mixing (keeping the lowest energy CF exciton), CF diagonalization produces explicit wave functions which, when tested against exact wave function, are found to be excellent approximations to the ground states, thus demonstrating that Λ L mixing captures the physics of the second LL FQHE. This will be seen to be the case for the entire filling factor range where the second LL behaves differently from the lowest LL. In particular, for $\nu^{(1)} = 1/3$, the overlap with the exact wave function increases from 0.71 to 0.95 (for six particles in the disk geometry) upon lowest-order Λ L mixing.

The Λ L mixing caused by the residual inter-CF interactions has been studied through CF diagonalization previously in various other contexts, for example the quantum dot states²⁸, the Luttinger liquid at the edge of the FQHE²⁹, the stability of the FQH liquid state against CF excitons³⁰, and for obtaining improved variational bounds for the FQHE ground state energies in the lowest LL³¹. It has quantitative, and sometimes even qualitative consequences.

The plan of the rest of the paper is as follows. The next section shows, by comparison of the exact ground states in the lowest, the second and the third Landau levels for six electrons on a disk, that there exists a filling factor range where they behave differently. Sec. III will outline the method of CF diagonalization, which incorporates the inter-CF interactions through Λ L mixing. Sec. IV will include the effect of Λ L mixing at the lowest order to obtain modified variational ground states in the second LL, and find high overlaps, between 0.94 and 0.98, with the exact ground state. We then proceed to use the

same method in the spherical geometry to estimate the excitation gap at $\nu^{(1)} = 1/3$ in Sec. V.

II. EXACT DIAGONALIZATION

A. Basics

The Hamiltonian for the 2DES is

$$\begin{aligned} H &= H_K + H_I + g\mu\mathbf{B} \cdot \mathbf{S}; \\ H_K &= \frac{1}{2m_b} \sum_j \left(\mathbf{p}_j + \frac{e}{c} \mathbf{A}(\mathbf{r}_j) \right)^2, \\ H_I &= \frac{e^2}{\epsilon} \sum_{i < j} \frac{1}{|\mathbf{r}_i - \mathbf{r}_j|}, \end{aligned} \quad (1)$$

where m_b is the band mass of the electron and ϵ is the dielectric constant of the host semiconductor. We use complex coordinates $z = x - iy$ on the plane and a symmetric gauge vector potential $\mathbf{A} = (-By/2, Bx/2, 0)$. The distance will be measured in units of the magnetic length $l_B = \sqrt{\hbar c/eB}$ and interaction energy in units of $e^2/\epsilon l_B$. The angular momentum J_z commutes with both H_K and H_I , and the eigenfunctions of J_z and H_K may be written as

$$\psi_{n,l}(z) = \frac{1}{\sqrt{2\pi n! l!}} (a^\dagger)^n (b^\dagger)^l \exp\left(-\frac{|z|^2}{4}\right), \quad (2)$$

where the lowering operators are defined as

$$a = \frac{\alpha + \beta}{\sqrt{2}}, \quad b = \frac{\alpha^\dagger - \beta^\dagger}{\sqrt{2}} \quad (3)$$

$$\alpha = \frac{z}{2}, \quad \beta = \partial_x + i\partial_y = 2\partial_{z^*} \quad (4)$$

In terms of the raising and lowering operators, the kinetic energy part of the Hamiltonian is given by

$$H_K = \left(a^\dagger a + \frac{1}{2} \right) \hbar\omega_c, \quad (5)$$

with $\omega_c = eB/m_b c$, and the angular momentum operator is $J_z = b^\dagger b - a^\dagger a$. The LL index is n , and the angular momentum is $l - n$. The Slater determinants of states given in Eq. (2) are used as basis vectors when H_I is diagonalized in a finite subspace of the Hilbert space.

We will neglect LL mixing throughout this paper, which is a good approximation when the interaction strength is small compared to the cyclotron energy, and also restrict ourselves to states which are maximally spin polarized (i.e. fully spin polarized in the topmost partially filled Landau level); therefore the last term in Eq. (1) (the Zeeman term) can be dropped. The exact diagonalization will be carried out in each L sector separately, where L is the total angular momentum of

electrons, because the Coulomb interaction does not mix states with different L . Fixing the total L confines the electrons to a disk (hence the name ‘‘disk geometry’’). The filling factor can be tuned by varying L . The filling factor is not really a well-defined quantity for a finite system, and finite systems do not necessarily represent a thermodynamic system with a well-defined filling factor. For certain wave functions it is possible to write a relation between L and ν for a finite N . Laughlin’s wave function³² for $\nu = 1/(2p+1)$ (where p is integer) satisfies the relation

$$\frac{1}{2p+1} = \binom{N}{2} \frac{1}{L}. \quad (6)$$

We thus know what L value corresponds to $\nu = 1/(2p+1)$ in the disk geometry, and it is natural to assume that the filling factor decreases monotonically with L .

Two-body interactions in the lowest LL are characterized by the Haldane pseudopotentials^{10,33} V_m , which are the energies of two electrons in relative angular momentum m state, $|\psi_m\rangle$,

$$\begin{aligned} V_m &= \frac{\langle \psi_m | V(z_1 - z_2) | \psi_m \rangle}{\langle \psi_m | \psi_m \rangle} \\ &= \frac{1}{2^{2m+1} m!} \int r dr V(r) r^{2m} e^{-r^2/4} \\ &= \int q dq \tilde{V}(q) L_m(q^2) e^{-q^2}, \end{aligned} \quad (7)$$

where $V(\mathbf{r}) = 1/r$ is the Coulomb interaction, $\tilde{V}(q)$ is its Fourier transform, and L_m is a Laguerre polynomial. The interaction part of the Hamiltonian can be written in terms of the pseudopotentials:

$$H_I |\psi\rangle = \sum_{i < j} \sum_m V_m P_m^{ij} |\psi\rangle, \quad (9)$$

where P_m^{ij} projects the wave function of the i, j th particles into the state of relative angular momentum m . As the spatial part of the fermion wave functions is fully antisymmetric (full spin polarization is assumed), only the odd m channels are filled.

B. Comparing states in different Landau levels

When studying the state in n th LL we assume that the completely filled $0, \dots, (n-1)$ LL’s are inert, i.e., we diagonalize in the Hilbert subspace of the n th LL. The existence of LL raising operators in the planar geometry lets us map this problem to the lowest LL by using effective pseudopotentials V_m^n :

$$V_m^n = \frac{\langle \psi_m^n | V(z_1 - z_2) | \psi_m^n \rangle}{\langle \psi_m^n | \psi_m^n \rangle},$$

where $|\psi_m^n\rangle = (a^\dagger)^n |\psi_m\rangle$. One can show that

$$\tilde{V}^n(q) = (L_n(q^2/2))^2 \tilde{V}(q), \quad (10)$$

where $\tilde{V}^n(q)$ in the Fourier transform of the effective interaction for LL n . Then V_m^n can be calculated in a closed form by Eqs. (8) and (10) in a straightforward manner.

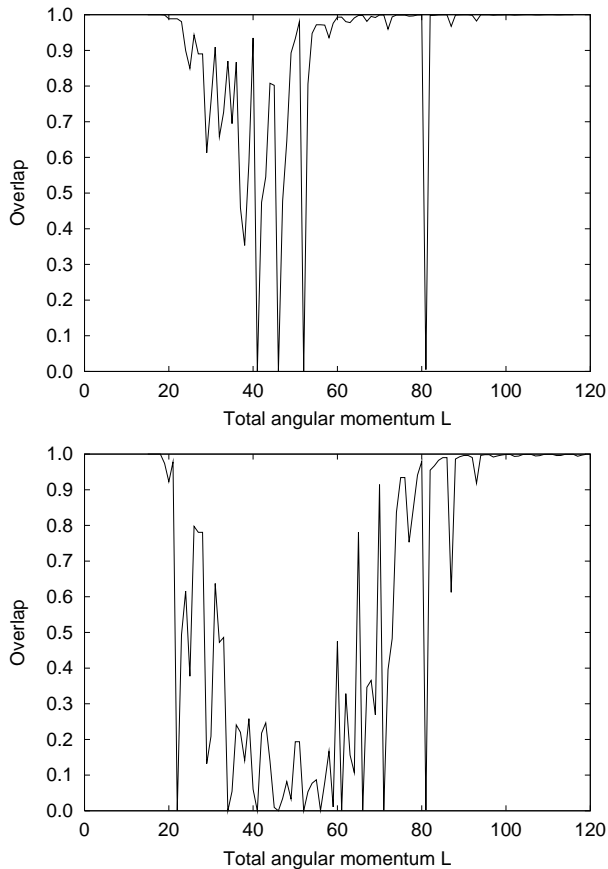


FIG. 1: Overlap of the LLL ground state $|\Psi_{ex}^{(0)}\rangle$ with the 2nd LL ground state $|\Psi_{ex}^{(1)}\rangle$ (top) and the 3rd LL ground state $|\Psi_{ex}^{(2)}\rangle$ (bottom) for $N = 6$. L denotes the total angular momentum. The overlap $|\langle\Psi_{ex}^{(0)}|\Psi_{ex}^{(1)}\rangle|$ is almost zero for $L = 41, 46, 52, 81$, and $|\langle\Psi_{ex}^{(0)}|\Psi_{ex}^{(2)}\rangle|$ nearly vanishes for $L = 22, 34, 41, 46, 52, 56, 61, 66, 71, 81$. The fillings $\nu = 1/3$ and $1/5$ occur at $L = 45$ and 60 , respectively. The lines are a guide to the eye.

Once we map the higher LL problem with a Coulomb interaction to a LLL problem with an effective interaction, we can work within the lowest LL, with different interactions simulating different LL's. This is what we will do. In the remainder of the article, the phrase “the ground state in the n th LL” will really mean “lowest LL sibling of the n th LL ground state.” Of course, the actual n th level ground state can be obtained from the lowest LL wave function by promoting it to the n th LL using the raising operators. With that understanding, the ground states $|\Psi_{ex}^{(n)}\rangle$ of different LL's can be compared by calculating the overlap $\langle\Psi_{ex}^{(n)}|\Psi_{ex}^{(n')}\rangle$. (Of course, the real n th LL ground state for $n > 0$ is orthogonal to the LLL ground state.)

Fig. 1 shows how the overlap between the second and

lowest (upper panel) and the third and lowest (lower panel) Landau levels varies with L . It is apparent that there is an angular momentum range where the ground states in the lowest and the excited LL's are quite different. As one considers higher LL's, the range of this region widens. Similar behavior is found for $N = 7$ and $N = 8$; see Figs. 2 and 3.

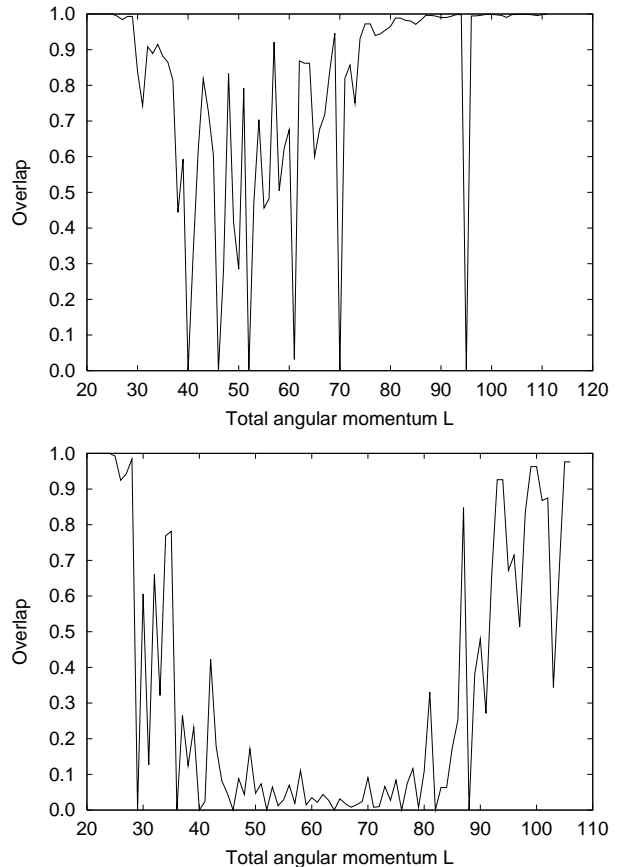


FIG. 2: Overlap of the LLL ground state $|\Psi_{ex}^{(0)}\rangle$ with the 2nd LL ground state $|\Psi_{ex}^{(1)}\rangle$ (top) and the 3rd LL ground state $|\Psi_{ex}^{(2)}\rangle$ (bottom) for $N = 7$. The overlap $|\langle\Psi_{ex}^{(0)}|\Psi_{ex}^{(1)}\rangle|$ is near zero for $L = 40, 46, 52, 70, 95$ and quite low (≈ 0.03) for $L = 61$, where L is the total angular momentum. The overlap $|\langle\Psi_{ex}^{(0)}|\Psi_{ex}^{(2)}\rangle|$ is rather low over a range of L . The fillings $\nu = 1/3$ and $1/5$ correspond to $L = 63$ and 105 , respectively. The lines are a guide to the eye.

There are angular momenta where the ground states in different Landau levels are nearly orthogonal. For example, for $N = 6$ $|\langle\Psi_{ex}^{(1)}|\Psi_{ex}^{(0)}\rangle| = 0.00024, 0.005$ for $L = 41, 81$, respectively, and is 0 within numerical accuracy for $L = 46, 52$. This near orthogonality is most unexpected. We have found that, in most cases, the following simple explanation can be given for it. As known from quantum dot studies^{28,34}, two-dimensional few electron systems in a strong transverse magnetic field have a tendency to form crystallites. Crystallite structures with $N = 6$ fall into two classes of symmetry: the (1,5) crystallite resembles a rotating molecule with one particle

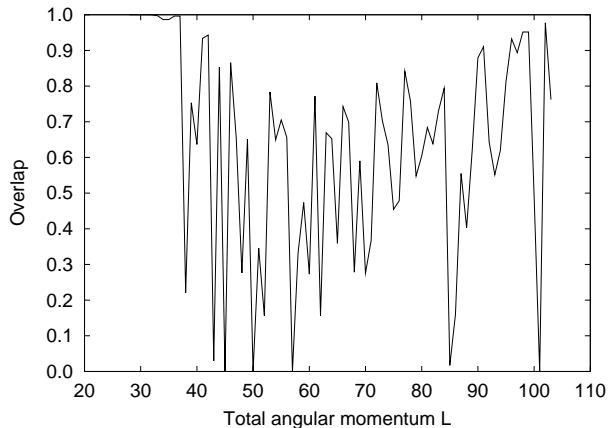


FIG. 3: Overlap of the LLL ground state $|\Psi_{ex}^{(0)}\rangle$ with the 2nd LL ground state $|\Psi_{ex}^{(1)}\rangle$ for $N = 8$ particles. The overlap $|\langle\Psi_{ex}^{(0)}|\Psi_{ex}^{(1)}\rangle|$ is almost zero for $L = 45, 50, 57, 85, 101$, where L is the total angular momentum. The fillings $\nu = 1/3$ and $1/5$ occur at $L = 84$ and 140 , respectively. The lines are a guide to the eye.

at the center and five in a ring; the (0,6) crystallite has all particles on a ring. Although the density profile differentiates between the two groups, the pair correlation function contains more information about the crystallite structure. For $N = 6$ and $L = 41, 46, 52, 81$ the symmetry of the crystallites in the two LL's differ, as suggested by the “effective” density profiles $\rho^{\text{eff}}(r)$ in Fig. 4 and demonstrated by the pair correlation functions $g^{\text{eff}}(\mathbf{r})$ in Fig. 5. (The superscript “eff” reminds us that the density or the pair correlation function are for the lowest LL representation of the n th LL states. The “real” density or the pair correlation function in the n th LL can be obtained by elevating the wave functions to the n th LL with the help of the raising operators.) For $L = 41$ and $L = 46$ the crystallite in the LLL has (1,5) symmetry while the one in the 2nd LL has (0,6) symmetry; for $L = 52$ and $L = 81$ the opposite holds. Although the majority of cases of almost zero overlap can be understood this way, there are exceptions ($N = 7, L = 95$ and $N = 8, L = 101$). We have not explored this issue further.

Outside a range of L , the higher LL physics is similar to that in the lowest LL. It was shown earlier^{11,35} that for $\nu \leq 1/5$ the lowest two LL's should show similar behavior. The difference at $N = 6, L = 81$ seems to violate this rule, but the system is so small that this exception can be attributed to finite size effects. We have found no such exception for $N = 7$ in the L range that we have investigated below $\nu = 1/5$ ($105 < L \leq 111$); for $N \geq 8$ the total angular momentum corresponding to $\nu = 1/5$ could not be reached.

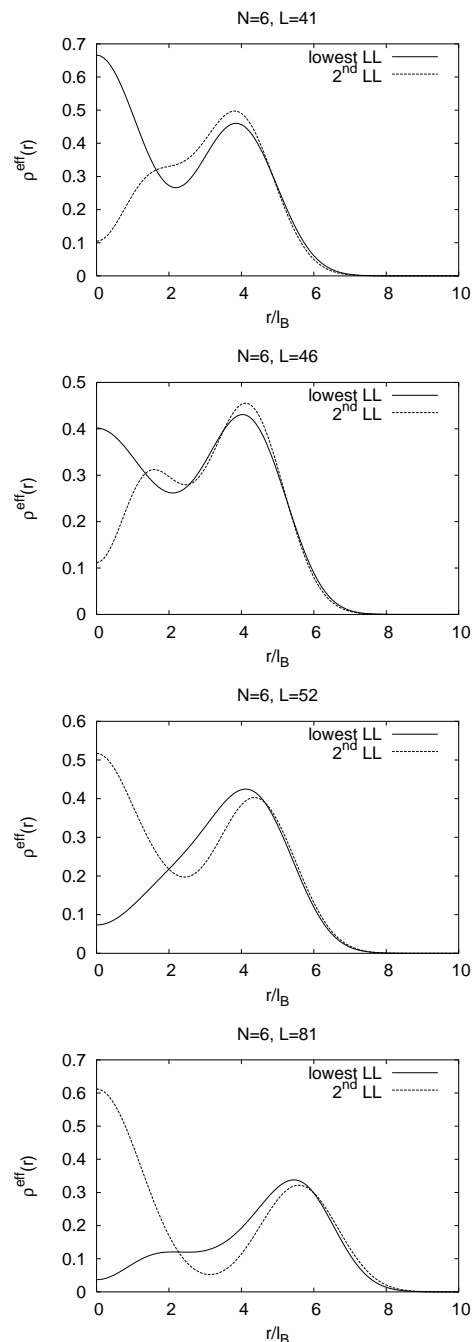


FIG. 4: Comparison of the density profiles $\rho^{\text{eff}}(r)$ of the exact lowest LL and 2nd LL ground states for the angular momentum (L) values for which the overlap between the two states is nearly zero. The reason for the superscript “eff” is that the density is calculated for the lowest LL sibling of the actual ground state. Note the different behaviors near the origin. The two Landau levels prefer crystallites with different symmetries at these L values. The distance is measured in units of l_B , the magnetic length.

III. CF DIAGONALIZATION

The idea of composite fermion diagonalization is conceptually quite straightforward. Instead of diagonalizing in the full LLL basis space, as is done in exact diagonalization studies, we diagonalize the full Hamiltonian in a restricted basis of correlated states produced by the CF theory. The correlated basis is constructed as follows. The CF theory^{3,4} maps interacting electrons at L into non-interacting fermions at L^* (taking, for concreteness, the disk geometry),

$$L^* = L - pN(N - 1). \quad (11)$$

We begin with the Slater determinant states $\Phi_\alpha^{L^*}$, which are some low kinetic energy states at L^* (chosen as explained below), and construct Jain's wave functions as:

$$\Psi_\alpha^L = \mathcal{P}_{LLL} \Phi_1^{2p} \Phi_\alpha^{L^*}, \quad (12)$$

where Φ_1 is the wave function at $\nu = 1$ and \mathcal{P}_{LLL} projects the state to the lowest LL. In the planar geometry,

$$\Phi_1^{2p} = \prod_{j < k} (z_j - z_k)^{2p}. \quad (13)$$

(The form for Φ_1 in the spherical geometry is given later.) The mapping in Eq. (12) amounts to a description of the 2DES in terms of composite fermions, consisting of the bound state of an electron with $2p$ quantized vortices of the 2DES wave function. ^{2p}CF denotes a CF with flavor $2p$. The LL's at L^* become ΛL 's of composite fermions under the above mapping, and the cyclotron energy at L^* becomes the effective cyclotron energy of CF's. While the diagonalization in the basis defined by Ψ_α^L is in principle straightforward, its actual implementation requires several technically challenging steps which have all been demonstrated previously. The lowest LL projection will be evaluated following Jain and Kamilla⁴. The states Ψ_α^L are not necessarily orthogonal; their orthogonalization and the diagonalization of the Hamiltonian matrix requires the evaluation of large dimensional integrals. Mandal and Jain²⁹ have demonstrated how this can be carried through in a Monte Carlo scheme. We note that Monte Carlo is used only to evaluate integrals.

Next we come to the choice of the basis $\{\Phi_\alpha^{L^*}\}$ at L^* . Electrons at L^* will in general occupy several Landau levels, which map into ΛL 's of composite fermions through the above construction. At the simplest level (referred to as the zeroth order approximation), these basis states are chosen to be the distinct degenerate kinetic energy *ground* states of non-interacting fermions at L^* . The ΛL mixing corresponds to LL mixing of fermions at L^* , and can be incorporated into theory by considering a larger basis:

$$[\{\Phi_\alpha^{(0)}\}, \{\Phi_\beta^{(1)}\}, \{\Phi_\gamma^{(2)}\}, \dots, \{\Phi_\zeta^{(J)}\}], \quad (14)$$

where $\{\Phi_\eta^{(J)}\}$ represents all η basis wave functions at L^* with kinetic energy J (in units of the cyclotron energy)

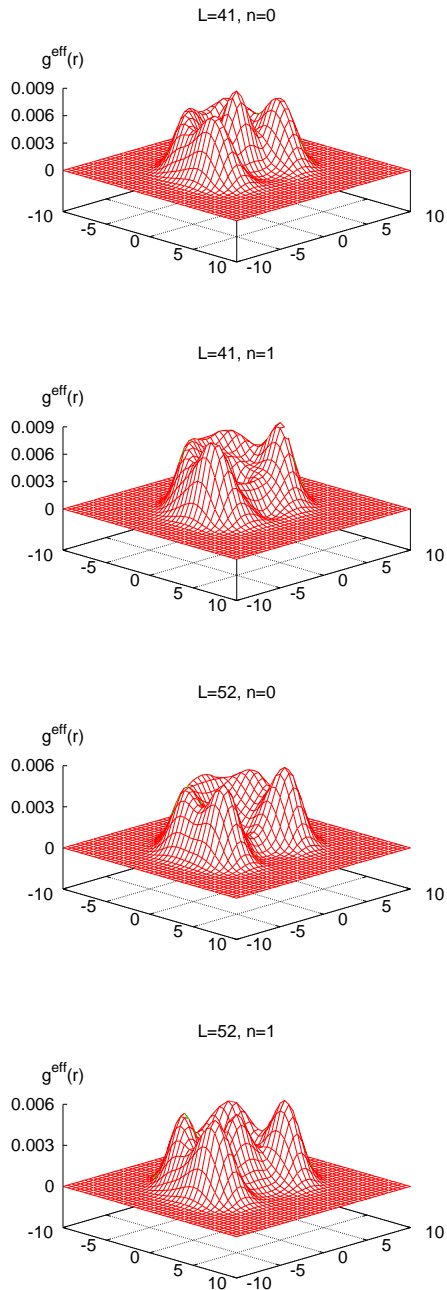


FIG. 5: The “effective” pair correlation function $g^{\text{eff}}(\mathbf{r})$ of the ground state for total angular momenta $L = 41$ and $L = 52$ in the lowest ($n = 0$) and the second ($n = 1$) Landau levels. The distance \mathbf{r} is measured from the center of the disk in units of the magnetic length l_B . The reason for the superscript “eff” is that the pair correlation function is calculated for the lowest LL sibling of the actual higher LL ground state. Similar differences were found for $L = 46$ and $L = 81$.

relative to the ground state kinetic energy. The corresponding CF basis is given by

$$\{ \{ \Psi_\alpha^{(0)} \}, \{ \Psi_\beta^{(1)} \}, \{ \Psi_\gamma^{(2)} \}, \dots, \{ \Psi_\zeta^{(J)} \} \}, \quad (15)$$

with $\Psi_\eta^{(j)} = P_{LLL} \Phi_1^{2p} \Phi_\eta^{(j)}$. A diagonalization in this basis incorporates the effect of ΛL mixing perturbatively. Fig. 6 explains the physics pictorially. We will denote by $\chi^{(J)}$ and $E^{(J)}$ the ground state wave function and the ground state energy obtained by CF diagonalization. In the spherical geometry, $E^{(J)}(L)$ and $\chi^{(J)}(L)$ will refer to the ground state energy and its wave function obtained by CF diagonalization in the orbital angular momentum L sector. As with all variational wave functions the energy $E^{(J)}$ is a strict upper bound on the exact energy.

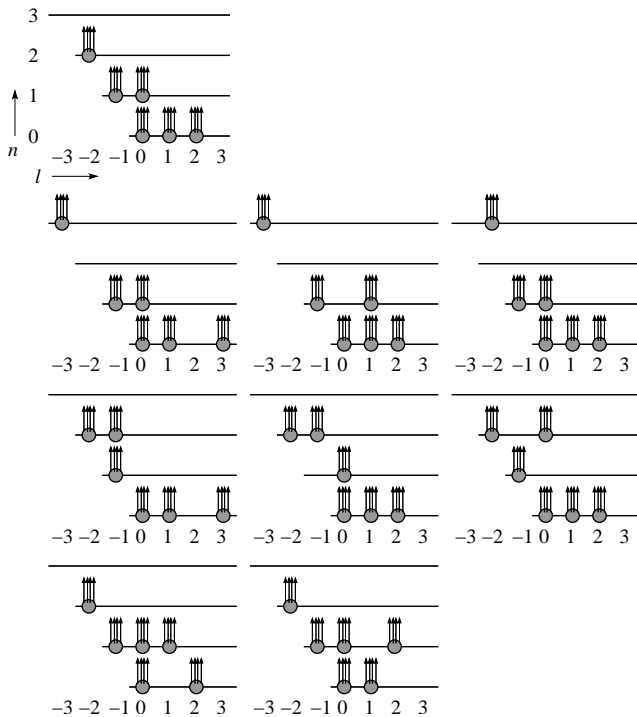


FIG. 6: The CF basis states (schematically) for $N = 6$ electron system at $L = 60$, which maps into $L^* = L - 2N(N-1) = 0$ of ${}^4\text{CF}$'s (composite fermions carrying four quantized vortices). The y-axis shows the ΛL index, and the x-axis shows the angular momentum index. The top row shows the state with the smallest effective cyclotron energy; there is only one state at that energy. The remaining figures show all the linearly independent configurations with one additional unit of kinetic energy. (There are a total of 10 distinct electron states in the $J = 1$ basis at L^* , which produce 9 linearly independent CF basis states.)

Of course, by increasing J , one will eventually obtain the exact state (although through an unnecessarily complicated route). The great advantage of the CF theory is that a very good approximation to the exact state is obtained by diagonalizing in a very small basis, in addition to providing an understanding of the physics. For many total angular momenta L a unique state is obtained at

the lowest level (i.e. $\Phi^{(0)}$ is unique), which gives a variational state with no free parameters. In the spherical geometry used in Sec. V this happens only when ν^* is an integer. On the disk there are many such states (c.f. Table II), labeled compact states³⁶.

The edge effects are significant in the disk geometry used in this section, while the spherical geometry used in Sec. V represents the bulk. In the spherical geometry, excitations are obtained by promoting a CF from the highest filled ΛL to the lowest empty ΛL , leaving behind a hole. Thus in $\Psi_\eta^{(J)}$, J CF particle-hole pairs exist. We will find the J th order variational state in the subspace spanned by CF states with $\leq J$ holes in the highest filled CF ΛL of $\Psi^{(0)}$. In the disk geometry, once a CF is raised to a higher ΛL , its angular momentum is no longer fixed, and one can redistribute the angular momenta of the particles in the lowest ΛL . This additional variational freedom lets us investigate edge effects as well.^{28,29}

Once the CF basis is constructed, one evaluates the overlaps $\langle \Psi_\alpha^{(j_1)} | \Psi_\beta^{(j_2)} \rangle$ between the basis vectors and the matrix elements of the interaction $\langle \Psi_\alpha^{(j_1)} | H_I | \Psi_\beta^{(j_2)} \rangle$ for $j_1, j_2 \leq J$ in the J th order using a Metropolis Monte Carlo technique. That requires the knowledge of the real-space interaction corresponding to the effective pseudopotentials V_m^n . The inverse Fourier transform of $\tilde{V}^n(q)$ in Eq. (10) is not defined, as the required integral is divergent. This, however, causes no problem. Because the pseudopotentials completely determine the interaction, any real-space interaction $V^n(r)$ that gives the same V_m^n through

$$V_m^n = \frac{\langle \psi_m | \sum_{i < j} V^n(z_i - z_j) | \psi_m \rangle}{\langle \psi_m | \psi_m \rangle}, \quad (16)$$

will be sufficient for our purposes. Thus we can use some convenient prescription for the analytic form of $V^n(r)$. The goal is that the Monte Carlo evaluation of the matrix elements of $V^n(r)$, required by the diagonalization in the correlated CF basis, should converge rapidly. In this paper we will use the following form:

$$V^{\text{eff}}(r) = \frac{1}{r} + \sum_{i=0}^M c_i r^i e^{-r}. \quad (17)$$

The form of the real-space interaction in Eq. (17) is based on the observation that the long-range behavior of the effective interaction should approach the Coulomb interaction, hence all corrections must be short-range. Keeping enough number of terms in the sum will give as accurate a representation of the interaction as desired. For our purposes, it is enough to keep the first seven terms ($M = 6$) in the sum. We calculate the first seven odd m pseudopotentials $V_1^{\text{eff}}, V_3^{\text{eff}}, \dots, V_{13}^{\text{eff}}$ from Eq. (17) symbolically by Mathematica, and determine c_i ($0 \leq i \leq M$) to satisfy

$$V_m^{\text{eff}} = V_m^1.$$

TABLE I: Coefficients in Eq. (17) to produce the effective interaction for the second LL.

| Coefficient | Value |
|-------------|-----------|
| c_0 | -50.36588 |
| c_1 | 87.38159 |
| c_2 | -56.08439 |
| c_3 | 17.76573 |
| c_4 | -2.97162 |
| c_5 | 0.25132 |
| c_6 | -0.008435 |

The coefficients c_i thus obtained, and used in our calculations below, are given in Table I, and the resulting real space interaction is shown in Fig. 7. Alternative prescriptions are available in the literature. Refs. 7,37,38 use a Gaussian functional form for the same purpose:

$$\frac{1}{r} + \sum_{i=0}^M c_i r^{2i} e^{-r^2}.$$

This form, however, is less convenient for our purposes, because it yields a real-space potential that oscillates strongly as a function of distance, causing an extremely slow convergence in Monte Carlo.

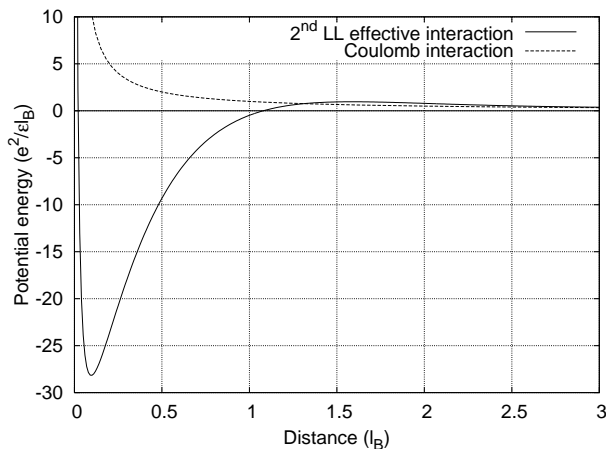


FIG. 7: The effective real-space potential $V^{\text{eff}}(r)$ (defined in Eq. 17) which simulates the second LL physics in the lowest LL. In spite of the deep dip at $r < l_B$, where l_B is the magnetic length, it reproduces the 2nd LL pseudopotentials to a very high accuracy (details in text).

We comment on the validity of the truncated interaction, i.e. Eq. (17) with $M = 6$ and the coefficients in Table I. First, the physics of the FQHE is governed by the first few relevant pseudopotentials. Since our truncated interaction reproduces correctly, by construction, the first *seven* odd pseudopotentials, it is expected to be quite good. Second, V^{eff} is also guaranteed to reproduce the pseudopotentials for very large m , where the interaction approaches $1/r$. We have found that the largest

relative error in V_m is 5% at $m = 37$ up to $m \leq 49$. (For a given total angular momentum L , the greatest relative angular momentum is $m_{\text{max}} = L - \binom{N-1}{2}$; for our calculations, which go up to $L = 60$ for $N = 6$, the largest relevant relative angular momentum is 49.) At such large m , the pseudopotential is so small that such error is of no consequence. As a final test, we have compared the ground state of the truncated interaction with the ground state of the Coulomb interaction. In the $L \leq 75$ range the smallest overlap occurs at $L = 71$, which is 0.998303. To quote a typical number, at $L = 45$ the overlap is 0.99997. The truncated interaction is thus essentially exact.

The overlap and interaction matrix elements for the effective interaction were calculated by the Metropolis algorithm. Typically 6.6×10^7 to 7.5×10^7 Monte Carlo steps (MCS) were performed, where a MCS is defined as a number of iterations during which each particle coordinate is expected to be updated once. Averages and error bars were calculated from five independent runs. When a sufficient accuracy was reached, the standard Gram-Schmidt procedure was used to find an orthonormal basis (often telling us that not all of the vectors in the correlated CF basis were independent), and H_I was diagonalized.

IV. RESULTS

We have performed CF diagonalization in the $34 \leq L \leq 60$ range. This encompasses $\nu = 1/3$ (which occurs at $L = 45$). The flavors ${}^2\text{CF}$'s are used for $L \leq 48$, ${}^4\text{CF}$'s for $L \geq 49$. (This choice ensures the smallest CF basis.) The results are shown in Table II and Fig. 8. The zeroth-order variational energies and overlaps are given for all $34 \leq L \leq 60$. The first-order wave function is evaluated for all L 's except for $L = 43, 44$; for these cases the correlated CF basis is too big ($D^{(1)} = 83$ and 111, respectively) preventing an evaluation of the matrix elements of H_I with sufficient accuracy.

The principal result of our study, as seen in Table II and Fig. 8, is that the CF theory without ΛL mixing is not satisfactory, but very good agreement is obtained once ΛL mixing is incorporated at the lowest order. Let us consider a few specific cases.

At $\nu = 1/3$ ($L = 45$) the zeroth-order variational wave function $\chi^{(0)}$ is the Laughlin wave function, the energy of which ($E_{CF}^{(0)} = 3.0796(3)$) significantly overestimates the exact energy 3.05354. The overlap is 0.712(2), which is similar to the values that were found in the spherical geometry¹¹. The first-order CF diagonalization yields $E_{CF}^{(1)} = 3.0621(1)$ and $|\langle \Psi_{ex} | \chi^{(1)} \rangle| = 0.9467(8)$.

We commented earlier that for certain L values the ground states of different LL's have anomalously low overlaps. Let us consider $L = 41, 46$, and 52 for $N = 6$. (We could not investigate $L = 81$ due to computational limitations.) At the zeroth order (i.e., without ΛL mixing), the overlaps for these L are $|\langle \Psi_{ex} | \chi^{(0)} \rangle| = 0.614(2)$, 0.004(2) and 0.933(7), respectively. For $L = 46$ the small

TABLE II: Comparison of the energies (in units of $e^2/\epsilon l_B$) of the exact ground state and the states obtained from 0th and 1st order CF diagonalization³⁹. The number in parentheses is the error in the last digit. D_{ex} , $D_{CF}^{(0)}$ and $D_{CF}^{(1)}$ are the dimensions of the full Hilbert space, of the CF basis in the 0th order calculation, and of the CF basis in the 1st order calculations, respectively. The 1st order energy was not calculated for $L = 43, 44$ because $D_{CF}^{(1)}$ is very large, which makes the numerical calculation very time consuming.

| L | E_{ex} | $E_{CF}^{(0)}$ | $E_{CF}^{(1)}$ | D_{ex} | $D_{CF}^{(0)}$ | $D_{CF}^{(1)}$ |
|-----|----------|----------------|----------------|----------|----------------|----------------|
| 34 | 3.57207 | 3.5801(1) | 3.5748(7) | 235 | 4 | 27 |
| 35 | 3.48739 | 3.5144(1) | 3.49786(2) | 282 | 1 | 10 |
| 36 | 3.44351 | 3.47805(2) | 3.4476(2) | 331 | 2 | 18 |
| 37 | 3.39199 | 3.42079(1) | 3.3962(1) | 391 | 5 | 31 |
| 38 | 3.37222 | 3.3899(3) | 3.3770(5) | 454 | 9 | 47 |
| 39 | 3.31020 | 3.3403(1) | 3.3174(3) | 532 | 1 | 17 |
| 40 | 3.25712 | 3.27476(2) | 3.2616(1) | 612 | 2 | 26 |
| 41 | 3.22851 | 3.2647(3) | 3.2330(5) | 709 | 4 | 41 |
| 42 | 3.18755 | 3.2206(3) | 3.1933(9) | 811 | 7 | 59 |
| 43 | 3.15253 | 3.1761(1) | - | 931 | 12 | 83 |
| 44 | 3.12831 | 3.1379(4) | - | 1057 | 18 | 111 |
| 45 | 3.05354 | 3.0796(3) | 3.0621(1) | 1206 | 1 | 28 |
| 46 | 3.04126 | 3.0805(5) | 3.0484(6) | 1360 | 1 | 39 |
| 47 | 3.01108 | 3.0561(3) | 3.0235(5) | 1540 | 2 | 55 |
| 48 | 2.97252 | 3.02019(8) | 2.9860(8) | 1729 | 3 | 74 |
| 49 | 2.94205 | 2.94937(4) | 2.9443(2) | 1945 | 4 | 46 |
| 50 | 2.87713 | 2.88772(2) | 2.8805(2) | 2172 | 2 | 32 |
| 51 | 2.87227 | 2.8786(6) | 2.8790(2) | 2432 | 1 | 19 |
| 52 | 2.85393 | 2.8667(3) | 2.8597(6) | 2702 | 10 | 65 |
| 53 | 2.82087 | 2.8375(3) | 2.827(1) | 3009 | 5 | 44 |
| 54 | 2.77835 | 2.79440(4) | 2.7881(5) | 3331 | 2 | 26 |
| 55 | 2.72364 | 2.737(2) | 2.7289(2) | 3692 | 1 | 13 |
| 56 | 2.72364 | 2.7457(2) | 2.7383(2) | 4070 | 5 | 39 |
| 57 | 2.69540 | 2.70221(2) | 2.7018(1) | 4494 | 2 | 21 |
| 58 | 2.68363 | 2.7054(7) | 2.6979(7) | 4935 | 9 | 48 |
| 59 | 2.64022 | 2.65914(2) | 2.6495(6) | 5427 | 3 | 25 |
| 60 | 2.58918 | 2.603(7) | 2.6034(4) | 5942 | 1 | 9 |

overlap follows because the 0th order CF basis contains only one state, which is very close to the LLL ground state. In the other two cases, the 0th order CF basis is larger (with 4 and 10 states); the greater flexibility results in better overlaps. With AL mixing, the overlaps increase to $|\langle \Psi_{ex} | \chi^{(1)} \rangle| = 0.9814(2)$, $0.9695(7)$ and $0.987(7)$, respectively.

V. ESTIMATION OF THE GAP AT $\nu^{(1)} = 1/3$

As was mentioned above, the existence of an excitation gap is crucial for the theoretical explanation of the phenomena of the FQHE. The best estimate so far is from

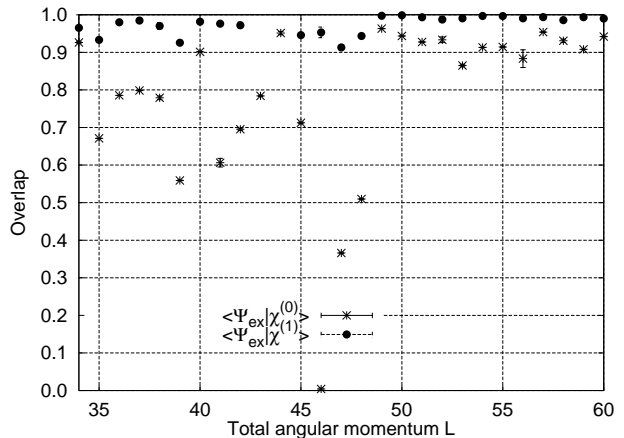


FIG. 8: Overlap of the exact 2nd Landau level ground state with the wave function obtained from CF diagonalization with and without AL mixing (solid circles and stars, respectively).

the exact diagonalization calculation of Morf²², where he obtained a gap of $\Delta_{7/3} \approx 0.02e^2/\epsilon l_B$ for $N = 10$ particles at $\nu^{(1)} = 1/3$, which gives a measure of the thermodynamic gap. In this section we estimate the excitation gap at $\nu^{(1)} = 1/3$ from CF diagonalization, incorporating the residual interactions among CF's.

For the calculation of excitation gaps we switch to the spherical geometry, which is good for examining the bulk properties. In this geometry, electrons are constrained to move on the surface of a sphere and a radial magnetic field is produced by placing a magnetic monopole of strength Q at the center, where $2Q\phi_0$ is the magnetic flux through the surface of the sphere ($2Q$ is an integer according to Dirac's quantization condition.)

On the sphere the total *orbital* angular momentum L is a good quantum number. The ground state at $L = 0$ is uniform and spherically symmetric and is considered incompressible if it is separated by a finite excitation gap from the other states.

The single particle states Y_{qlm} are called monopole harmonics⁴⁰ and are given by

$$Y_{qlm}(\Omega) = N_{qlm} (-1)^{l+m} e^{iq\phi} u^{q-m} v^{q+m} \times \sum_{s=0}^{l-q} \binom{l-q}{s} \binom{q+l}{l+m-s} \times (v^*v)^{l-q-s} (u^*u)^s, \quad (18)$$

where q is the monopole strength, $l = q + n$ is the single particle angular momentum where $n = 0, 1, \dots$ is the LL index, $m = -l, -l+1, \dots, l$ is the z-component of angular momentum, $\Omega = (\theta, \phi)$ is the position of the electron on the surface of the sphere in the usual coordinates, and $u \equiv \cos(\theta/2) \exp(-i\phi/2)$ and $v \equiv \sin(\theta/2) \exp(i\phi/2)$. The normalization coefficient is

$$N_{qlm} = \sqrt{\frac{2l+1}{4\pi} \frac{(l+m)!(l-m)!}{(l+q)!(l-q)!}}. \quad (19)$$

The degeneracy of the n th Λ -level is $2l + 1$ and the filling factor is defined as

$$\nu = \lim_{N \rightarrow \infty} \frac{N}{2Q}. \quad (20)$$

The distance between particles r_{ij} is taken to be the chord distance $r_{ij} = 2R|u_i v_j - v_i u_j|$ where the radius of the sphere is $R = \sqrt{Q}$ in units of magnetic length.

In the spherical geometry the CF wave function is written in the same form as in Eq. (12)

$$\Psi = P_{LLL} \Phi_1^{2p} \Phi,$$

where Φ is now a wave function for N non-interacting electrons at monopole strength q . Composite fermionization (vortex attachment) is again accomplished by multiplication of the Jastrow factor Φ_1^{2p} which in this geometry is written

$$\Phi_1^{2p} = \prod_{j < k} (u_j v_k - v_j u_k)^{2p} \quad (21)$$

Again, Φ_1 is the wave function of one filled LL. The projection P_{LLL} into the lowest LL in the spherical geometry is a complicated procedure and interested reader is again referred to the literature⁴. We then arrive at a wave function Ψ describing N electrons at $Q = q + p(N - 1)$.

To obtain states corresponding to the filling factors ($\nu = n/(2pn + 1)$) we create electron states at integral filling factors n . In the spherical geometry this amounts to setting the monopole strength to $2q = N/n - n$, the value corresponding to a total degeneracy of N . After attaching $2p$ vortices to each electron and projecting into the LLL we arrive at a wave function describing N interacting electrons at filling factor $\nu = n/(2pn + 1)$ called $\Psi^{(0)}$ (this wave function equivalently describes non-interacting CFs). As in the disk geometry $\Psi^{(0)}$ has been shown to be spectacularly accurate when compared with exact diagonalization results⁴. On the sphere $\Psi^{(0)}$ is a uniform state and exists only at $L = 0$. With no loss of generality we work within the z -component of angular momentum $L_z = 0$ subspace of the $2L + 1$ degenerate states in each L channel.

The low energy excited states $\Psi_\alpha^{(1)}$ are calculated as

$$\Psi_\alpha^{(1)} = P_{LLL} \Phi_1^{2p} \Phi_\alpha^{(1)}, \quad (22)$$

where $\Phi_\alpha^{(1)}$ represents the α states at $2q = N/n - n$ where one electron in the filled LL n has been allowed to occupy the LL $(n + 1)$ leaving behind a hole. In general $\Phi_\alpha^{(1)}$ is a superposition of Slater determinants. There is one state for each total angular momentum $L = 1, 2, \dots, (N + n^2 + n)/n$, so no CF diagonalization is required, though it has been shown⁴¹ that the application of P_{LLL} annihilates the state at $L = 1$.

The calculated excitation spectrum $E^{(1)}(L)$ for $\nu^{(1)} = 1/3$ for $N = 16$ is shown by solid circles in Fig. 9. (We are showing a system for $N = 16$ for illustrative purposes only; similar behavior occurs for other system sizes.) It

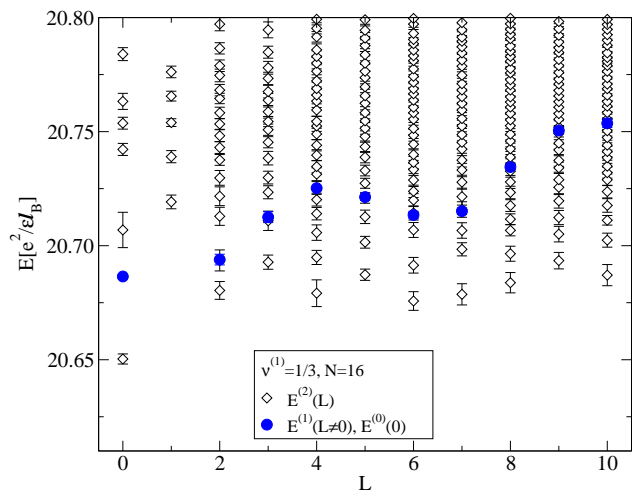


FIG. 9: (Color online) The open diamonds represent the energy spectra for the $J = 2$ basis as a function of total orbital angular momentum L , i.e. $E^{(2)}(L)$, while the blue circles represent the energy spectra using the $J = 1$ basis, i.e. $E^{(1)}(L \neq 0)$, at filling factor $\nu^{(1)} = 1/3$ for $N = 16$ electrons. The energies have been corrected for the finite sized deviation in the density by multiplication by $\sqrt{\rho/\rho_N} = \sqrt{2Q\nu/N}$. The contribution from the uniform positive background has not been subtracted.

has an $L = 0$ ground state ($\Psi^{(0)}$ in this case) separated from the other states by a gap. It may be tempting to go ahead and calculate the excitation gap, but we know that $\Psi^{(0)}$ is a poor representation of the actual ground state in the second LL from the studies of small systems in the spherical geometry¹¹ and in the disk geometry (this work and elsewhere⁴) and suspect that the excited states are also equally bad. Thus, we expand our basis for CF diagonalization (Eq. 15) to $J = 2$.

The open diamonds in Fig. 9 show the spectra when the interaction in Eq. (17) is diagonalized using the CF basis in Eq. (15) with $J = 2$ for $N = 16$ at $\nu^{(1)} = 1/3$. Two points are noteworthy. First, as expected, the lowest energy in each L sector has been lowered significantly. (Many new higher energy states are also created, but they are not of interest in this work.) Second, the gap is significantly enhanced. Both these underscore the importance of ΛL mixing for the second LL FQHE. Table III gives the overlap between $\chi^{(2)}$ at $L = 0$ and $\Psi^{(0)}$ for a number of system sizes. The relatively small overlaps give further evidence that the CF diagonalization in the $J = 2$ basis has significantly improved the ground state wave function.

The overall size of the basis diagonalized for $J = 1$ consists of $(N + n^2 + n)/n + 1$ states across the whole spectrum while the size of the basis diagonalized for $J = 2$ is approximately 500 states for $N = 16$ (9 states in the $L = 0$ channel up to ~ 50 states in the $L = 10$ channel.) That should be compared to the dimension of the subspace for the exact state which is $\sim 10^{10}$, making it inaccessible to exact diagonalization. The overlap and

TABLE III: The overlap between the improved variational ground state wave function and the Laughlin wave function at $\nu^{(1)} = 1/3$ ($\langle \chi^{(2)} | \Psi^{(0)} \rangle$) for $N = 10, 11, 12, 13$, and 16 . The number given in parentheses is the Monte Carlo uncertainty.

| N | $ \langle \chi^{(2)} \Psi^{(0)} \rangle ^2$ |
|-----|---|
| 10 | 0.82(1) |
| 11 | 0.81(1) |
| 12 | 0.82(2) |
| 13 | 0.835(3) |
| 16 | 0.77(4) |

interaction matrix elements needed for CF diagonalization used on average 10^7 Monte Carlo iterations. The error reported in each value is the standard deviation of the mean calculated between, on average, ten separate Monte Carlo configurations. Running in parallel on a multi-node computer cluster, approximately 7200 hours of computer time were utilized in the spherical geometry calculations. To obtain the final energy spectra we implement the Gram-Schmidt procedure to diagonalize the interaction Hamiltonian within the subspace spanned by the $J = 2$ basis as it is generally not orthogonal.

A technical detail regarding the sampling function is noteworthy. We choose this function to be one of the basis states that we feel closely represents the true state. In principle, in the limit of infinite Monte Carlo iterations the result calculated approaches the exact result regardless of sampling function. In practice, a proper choice of sampling function can make the Monte Carlo converge faster. Using the effective potential in Eq. (17) we have found that the Monte Carlo error is on the order of 10 times larger than the error when using the pure Coulomb potential when $\Psi^{(0)}$ is used as the sampling function. Consequently, we have calculated the spectra using many different sampling functions. Since we are only interested in the lowest energy in each L channel, this energy was chosen to be the energy with the smallest statistical error among the energies calculated with the different sampling functions.

We believe that $J = 2$ CF diagonalization is quantitatively accurate in the second LL, and proceed to calculate the excitation gap for FQHE at $\nu^{(1)} = 1/3$. Fig. 10 shows the energy gap Δ as a function of wave vector k , where $kl_B = L/R$. We have calculated the energy gap for $N = 10, 11, 12, 13$, and 16 represented by the different symbols. The energies for different system sizes have roughly collapsed onto a single line indicating that we are close to the thermodynamic limit. The Monte Carlo error is ~ 10 times what one is used to with gap calculations in the lowest LL, making the numbers less certain. However, many conclusions can still be reached.

The shape of Δ is somewhat different than that of the lowest LL $1/3$ state which shows one roton minimum. There seem to be two minima in the spectra, at $kl_B \sim 0.5$ and $kl_B \sim 1.25$. The value of roton gap at both

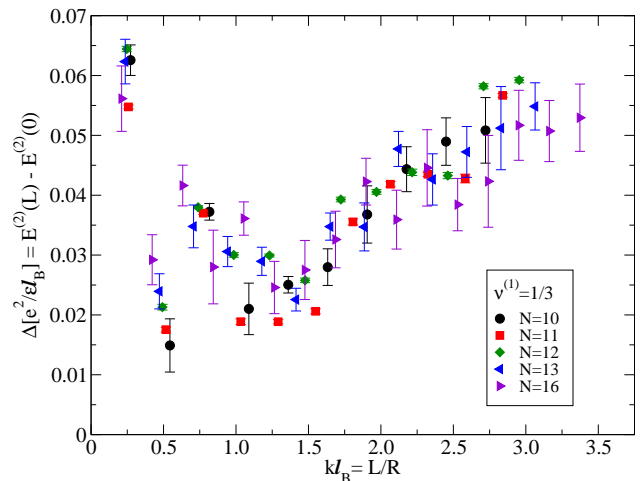


FIG. 10: (Color online) The different symbols represent the energy gap in units of $e^2/\epsilon l_B$ for systems sizes $N = 10, 11, 12, 13$, and 16 as a function of $kl_B = L/R$, where R is the radius of the sphere and L is the total orbital angular momentum. Each energy has been corrected for finite sized deviation in the density as in Fig. 9.

$kl_B \sim 0.5$ and $kl_B \sim 1.25$ is crudely $\sim 0.02e^2/\epsilon l_B$ in both cases. This is consistent with Morf's estimation²², further confirming that the CF theory with lowest order ΛL mixing is quite satisfactory for FQHE in the second LL. The transport gap is identified with the excitation energy at $L = N$ since in the thermodynamic limit this state describes an infinitely separated CF particle-hole pair; this is estimated to be $\sim 0.05e^2/\epsilon l_B$. The theoretical gaps are much larger than the gaps measured experimentally, however. In Ref. 42 the excitation gaps at $7/3$ and $8/3$ were measured as $\Delta_{7/3} = 0.10$ K and $\Delta_{8/3} = 0.055$ K, respectively. Using the experimental parameters our calculated gap for $\nu = 7/3$ is $\Delta \sim 2$ K for the roton and $\Delta \sim 5$ K for the transport gap. The theoretical calculations quite generally overestimate the FQHE gap; we expect that our estimate would scale down once finite thickness, LL mixing, and disorder effects are taken into account. In this context, it may be noted that the theoretical gap at $\nu = 5/2$ estimated from exact diagonalization studies by Morf²², $\Delta_{5/2} \approx 0.05e^2/\epsilon l_B$, corresponding to ~ 5 K, is also large compared to the experimental gap⁴² (~ 0.11 K).

In principle, our method allows one to obtain the excitation gap for fillings of the form $\nu^{(1)} = n/(2pn + 1)$. However, in practice we find that the Monte Carlo error is too large for any reasonable number of iterations, perhaps due to the nature of the effective potential (Eq. 17) at short distances and the smallness of the gap.

VI. CONCLUSION

We have shown that the residual interaction between CF's accounts for the deviation of 2nd LL FQHE states

and the LLL FQHE states in certain range of filling factors. This interaction can be taken into account by allowing for AL mixing, i.e., letting the ground state hybridize with CF particle-hole excitations across AL's, which is caused by the inter-CF interactions. The lowest level incorporation of AL mixing produces an excellent account of the second LL ground states. We also estimate the excitation gap at $\nu^{(1)} = 1/3$ and find that AL mixing strongly renormalizes it upwards.

Acknowledgments

We are indebted to Chia-Chen Chang for useful discussions and for sharing with us several numerical codes

he developed in other projects. We are grateful to the High Performance Computing (HPC) group at Penn State University ASET (Academic Services and Emerging Technologies) for assistance and computing time on the Lion-XL and Lion-XO clusters. Partial support of this research by the National Science Foundation under grants No. DMR-0240458 and DGE-9987589 (IGERT) is gratefully acknowledged.

-
- ¹ K. von Klitzing, G. Dorda, and M. Pepper, Phys. Rev. Lett. **45**, 494 (1980).
- ² D.C. Tsui, H.L. Stormer, and A.C. Gossard, Phys. Rev. Lett. **48**, 1559 (1982).
- ³ J.K. Jain, Phys. Rev. Lett. **63**, 199 (1989); Physics Today **53**(4), 39 (2000).
- ⁴ J.K. Jain and R.K. Kamilla, Int. J. Mod. Phys. **B11**, 2621 (1997); Phys. Rev. B **55**, R4895 (1997).
- ⁵ J.S. Xia, W. Pan, C.L. Vicente, E.D. Adams, N.S. Sullivan, H.L. Stormer, D.C. Tsui, L.N. Pfeiffer, K.W. Baldwin and K.W. West, Phys. Rev. Lett. **93**, 176809 (2004).
- ⁶ G. Gervais, L.W. Engel, H.L. Stormer, D.C. Tsui, K.W. Baldwin, K.W. West, and L.N. Pfeiffer, Phys. Rev. Lett. **93**, 266804 (2004).
- ⁷ V.W. Scarola, K. Park, and J.K. Jain, Phys. Rev. B **62**, R16259 (2000).
- ⁸ A.A. Koulakov, M.M. Fogler, and B.I. Shklovskii, Phys. Rev. Lett. **76**, 499 (1996).
- ⁹ J.P. Eisenstein, K.B. Cooper, L.N. Pfeiffer, and K.W. West, Phys. Rev. Lett. **88**, 076801 (2002).
- ¹⁰ F.D.M. Haldane in *The Quantum Hall Effect*, edited by S.M. Girvin (Springer, New York, 1987).
- ¹¹ N. d'Ambrumenil and A.M. Reynolds, J. Phys. C: Solid State Phys. **21**, 119 (1988).
- ¹² A.H. MacDonald, Phys. Rev. B **30**, 3550 (1984).
- ¹³ W. Pan, H.L. Stormer, D.C. Tsui, L.N. Pfeiffer, K.W. Baldwin, and K.W. West, Phys. Rev. Lett. **90**, 016801 (2003).
- ¹⁴ J.K. Jain, Phys. Rev. B **40**, 8079 (1989); Phys. Rev. B **41**, 7653 (1990).
- ¹⁵ K. Park and J.K. Jain, Phys. Rev. B **62**, R13274 (2000).
- ¹⁶ C-C. Chang and J.K. Jain, Phys. Rev. Lett. **92**, 196806 (2004).
- ¹⁷ A. Lopez and E. Fradkin, Phys. Rev. B **69**, 155322 (2004).
- ¹⁸ M.O. Goerbig, P. Lederer, and C. Morais-Smith, Phys. Rev. B **69**, 155324 (2004).
- ¹⁹ A. Wójs, Phys. Rev. B **63**, 125312 (2001); A. Wójs and J.J. Quinn, Physica E **12**, 63 (2002).
- ²⁰ R. Willett, J.P. Eisenstein, H.L. Stormer, D.C. Tsui, A.C. Gossard, and J.H. English, Phys. Rev. Lett. **59**, 1776 (1987).
- ²¹ M. Greiter, X.G. Wen, and F. Wilczek, Phys. Rev. Lett. **66**, 3205 (1991).
- ²² R.H. Morf, Phys. Rev. Lett. **80**, 1505 (1998);
- ²³ E.H. Rezayi and F.D.M. Haldane, Phys. Rev. Lett. **84**, 4685 (2000).
- ²⁴ V.W. Scarola, K. Park, and J.K. Jain, Nature **406**, 863 (2000).
- ²⁵ G. Moore and N. Read, Nucl. Phys. B **360**, 362 (1991).
- ²⁶ M.O. Goerbig, P. Lederer, and C. Morais-Smith, Phys. Rev. B **69**, 115327 (2004).
- ²⁷ G. Murthy and R. Shankar, Rev. Mod. Phys. **75**, 1101 (2003).
- ²⁸ G.S. Jeon, C-C. Chang, and J.K. Jain, Phys. Rev. B **69**, 241304(R) (2004); J. Phys: Condens. Matter **16**, L271 (2004).
- ²⁹ S.S. Mandal and J.K. Jain, Solid State Commun. **118**, 503 (2001); Phys. Rev. Lett. **89**, 096801 (2002).
- ³⁰ M.R. Peterson and J.K. Jain, Phys. Rev. B **68**, 195310 (2003).
- ³¹ S.S. Mandal, M.R. Peterson, and J.K. Jain, Phys. Rev. Lett. **90**, 106403 (2003).
- ³² R.B. Laughlin, Phys. Rev. Lett. **50**, 1395 (1983).
- ³³ F.D.M. Haldane, Phys. Rev. Lett. **51**, 605 (1983).
- ³⁴ T. Seki, Y. Kuramoto and T. Nishino, J. Phys. Soc. Jpn. **65**, 3945 (1996); P.A. Maksym, Phys. Rev. B **53**, 10879 (1996); W.Y. Ruan, Y.Y. Liu, C.G. Bao and Z.Q. Zhang, *ibid.* **51**, R7942 (1995); C. Yannouleas and U. Landman, *ibid.* **68**, 035326 (2003).
- ³⁵ A.H. MacDonald and S.M. Girvin, Phys. Rev. B **33**, 4009 (1986).
- ³⁶ J.K. Jain and T. Kawamura, Europhys. Lett. **29**, 321 (1995).
- ³⁷ S.-Y. Lee, V.W. Scarola, and J.K. Jain, Phys. Rev. B **66**, 085336 (2002).
- ³⁸ K. Park, V. Melik-Alaverdian, N.E. Bonesteel, and J.K. Jain, Phys. Rev. B **58**, R10167 (1998).
- ³⁹ We are using the Coulomb interaction for the exact calculation and the truncated interaction for the CF diagonalization. Even though they have almost identical pseudopotentials, sometimes the latter produces a very slightly lower energy than the energy of the exact ground state. To avoid confusion, the energies $E_{CF}^{(J)}$ in Table II are the expectation values of the second LL *Coulomb* interaction with respect to $\chi^{(J)}$.
- ⁴⁰ T.T. Wu and C.N. Yang, Nucl. Phys. **B107**, 365 (1976).

⁴¹ G. Dev and J.K. Jain, Phys. Rev. Lett. **69**, 2843 (1992).

⁴² W. Pan, J.-S. Xia, V. Shvarts, D.E. Adams, H.L. Stormer, D.C. Tsui, L.N. Pfeiffer, K.W. Baldwin and K.W. West,

Phys. Rev. Lett. **83**, 3530 (1999).

